Journal of Fluids and Structures 124 (2024) 104052

Contents lists available at ScienceDirect

Journal of Fluids and Structures

journal homepage: www.elsevier.com/locate/jfs

Passive control of flow-induced vibration of a sphere using a trip wire

Anchal Sareen [a,*], Kerry Hourigan [b], Mark C. Thompson [b]

[a] Department of Naval Architecture and Marine Engineering, Mechanical Engineering, University of Michigan, Ann Arbor, 48109, MI, USA
[b] Department of Mechanical and Aerospace Engineering, Monash University, Clayton, 3800, VIC, Australia

ARTICLE INFO

Keywords:
Fluid–structure interaction
Flow control
Wakes
Vortex streets

ABSTRACT

We experimentally investigated the potential of a trip wire as a passive control mechanism for controlling flow-induced vibration (FIV) of a three-dimensional bluff body. The effect of a surface trip wire was investigated for varying diameter ratio in the range $1.3\times10^{-2} \leqslant k/D \leqslant 6.7\times10^{-2}$, where k is the wire diameter and D is the sphere diameter, and trip-wire location in the range $20° \leq \phi \leq 60°$, where the angle ϕ was measured from the leading stagnation point. The FIV response of the sphere is characterised for a wide range of reduced velocities $3 \leqslant U^* \leqslant 20$, defined as $U^* = U/f_{nw}D$, where U is the free stream velocity and f_{nw} is the natural frequency of the system in water. It was found that for a fixed trip-wire diameter ratio, the vibration amplitude decreased progressively with increasing ϕ. Furthermore, the synchronisation regime became narrower, and the mode II and the plateau branches of the FIV response occurred for lower reduced velocities, compared to those for a smooth sphere. The control was highly effective for high reduced velocities ($U^* > 10$) with a maximum reduction of up to 97.8% for $\phi = 60°$. Interestingly, thicker trip wires ($k/D > 1.3\times10^{-2}$) were effective in disrupting Mode I, but induced a galloping-like response for higher reduced velocities. Tripping proved to be an effective passive control strategy for spheres, with the optimal trip-wire size varying across Mode I to Mode III.

1. Introduction

Flow over non-streamlined bodies, also known as bluff bodies, is a common occurrence in both natural and engineering contexts. Examples include offshore structures, automobiles, bridges, heat exchangers, aircrafts, tall buildings, and pipelines. At Reynolds numbers surpassing a critical threshold, the flow past these bluff bodies generates alternating vortices that can induce structural vibration known as flow-induced vibration (FIV). These vibrations occur across a wide range of Reynolds numbers and may result in severe structural fatigue and damage. Consequently, extensive research efforts over the past four decades have been dedicated to understanding the fundamental principles underlying these vibrations and effective means of suppressing them (e.g. Bearman, 1984; Blevins, 1990; Sarpkaya, 2004; Williamson and Govardhan, 2004; Païdoussis et al., 2010; Naudascher and Rockwell, 2012).

However, recently, there has been a rapidly growing interest in exploiting such large vibrations for harnessing renewable energy instead, driven by the urgent need to address the emerging climate crisis. A notable example of this is the recently developed Bladeless Wind Turbine prototype by the *Vortex Bladeless company* (vortexbladeless.com). This innovative device exploits the flow-induced vibration (FIV) of a oscillating cylinder to capture renewable energy from the wind. In the context of renewable energy applications, it is crucial to enhance these vibrations rather than suppress them in order to maximise energy output. This emphasises

* Corresponding author.
E-mail address: asareen@umich.edu (A. Sareen).

https://doi.org/10.1016/j.jfluidstructs.2023.104052
Received 8 August 2023; Received in revised form 11 December 2023; Accepted 16 December 2023
Available online 29 December 2023

the need of effective control strategies for manipulating the flow-induced vibrations that can either suppress these vibrations where it is undesirable, as in the case of offshore structures, or amplify them where they need to be enhanced, particularly in applications like renewable energy harvesting. Regardless of the application's objective, effective control of these vibrations requires a comprehensive understanding of the underlying fundamental principles leading to FIV. This study aims at understanding the fundamental principles of control of these flow-induced vibration of a sphere using a simple passive device of a trip wire.

Most prior fundamental work on the control of FIV is based on the canonical bluff-body geometry of a cylinder. In contrast, a sphere, which is the most basic 3D bluff-body prototype, exhibits intricate 3D wake structures and remains largely unexplored. Recently, there has been a significant advancement in our understanding and controlling of flow-induced vibration (FIV) of spheres under complex conditions (Sareen et al., 2018a,c,b, 2019; McQueen et al., 2020). These extensive experimental campaigns led to the discovery of new classes of FIV and coupled wake transitions, along with innovative approaches to actively control induced vibration of 3D bluff bodies. Although active control methods can provide effective control, they require external energy input and intricate control systems, making them less practical for certain applications. In contrast, passive control methods offer advantages such as simplicity, cost-effectiveness, and require no input power. However, there appears to be very few studies on passive control of FIV of spheres. Such methods, however, have been extensively investigated for the two-dimensional generic bluff body — the circular cylinder.

Passive control methods investigated for cylinders include surface modifications using roughness (Shih et al., 1993), dimples (Bearman and Harvey, 1993; Choi et al., 2006), helical wire (Lee and Kim, 1997), longitudinal grooves (Lim and Lee, 2002), splitter plates (Anderson and Szewczyk, 1997; Hwang et al., 2003; Kwon and Choi, 1996; Ozono, 1999), and small secondary control cylinder (Dalton et al., 2001; Sakamoto and Haniu, 1994; Strykowski and Sreenivasan, 1990). Among them, geometric modification in the spanwise direction near the separation point has been proven to be an effective strategy for drag reduction of the 2D body. Therefore, this 2D forcing mechanism has received much attention for passive drag reduction for cylinders. However, it is not clear if such methods can be directly translated to 3D geometries with more complex three-dimensional wakes, such as spheres (Choi et al., 2008).

For fixed spheres, boundary-layer control has proven effective for reducing drag. Boundary-layer control involves enhancing the near-wall tangential momentum in the boundary layer prior to flow separation so that the flow can overcome the adverse pressure gradient at the rear of sphere leading to delayed separation. This can be achieved either through inducing laminar-to-turbulent boundary-layer transition prior to separation, or through early laminar separation followed by immediate turbulent transition causing the flow to again reattach before the final separation further downstream (Choi et al., 2008). Direct boundary-layer transition can be achieved through surface roughness (Achenbach, 1972, 1974; Choi et al., 2006; Güven et al., 1980). In addition, early separation and reattachment before the main separation can be achieved through dimples or using a trip wire. Choi et al. (2006) showed that dimples on a sphere, such as golf-ball dimples, cause local flow separation and trigger shear layer instability along the separating shear layer, resulting in the generation of boundary-layer turbulence, reattachment to the sphere surface, and delay of the main separation. This process mimics that occurring in the drag crisis first reported in the seminal work of Achenbach (Achenbach, 1972, 1974).

Similar drag-reduction mechanisms can be found from controls using a trip wire located at the front surface of a bluff body (Choi et al., 2006; Maxworthy, 1969), and free-stream turbulence (Blackburn and Melbourne, 1996; Kiya et al., 1982). Son et al. (2011) investigated drag reduction of a fixed sphere at subcritical Reynolds numbers of $Re = 0.5 \times 10^5 - 2.8 \times 10^5$ (based on the free-stream velocity and sphere diameter). They varied the streamwise location of trip wire in the range 20°–70° from the stagnation point, and the diameter of the trip wire in the range $0.33 \times 10^{-2} < k/D < 1.33 \times 10^{-2}$. They reported different flow characteristics based on the diameter and size of the trip wire. For the lower Reynolds numbers, the disturbance created by the trip wire decayed downstream and there was no change to the position of the main separation. However, at higher Reynolds numbers, the presence of the trip wire delayed the main separation. When very thick trip wires were placed close to the separation, the trip wire promoted flow separation at the trip wire location itself, forming a relatively large recirculation zone at the rear of the trip wire. Fig. 1 shows a schematic of different flow patterns observed in the case of a bluff body. These flow patterns have been reported for spheres (Son et al., 2011; Deshpande et al., 2018) and cylinders (Igarashi, 1986; Behara and Mittal, 2011; Ekmekci and Rockwell, 2010; Alam et al., 2010) with trip wires. The existing research clearly shows that the characteristics of the boundary layer and main flow separation play a pivotal role in determining the forces acting on a sphere. Additionally, it suggests that the analysis of the boundary layer separation is sufficient to explain the control mechanism and that the precise quantification of the far wake structures may not be necessary. Even for an elastically-mounted bluff body undergoing flow-induced vibration, a recent study by Menon and Mittal (2021) revealed that while vortex shedding in the wake is necessary to initiate oscillations, it is the vorticity associated with the boundary layer over a bluff body that is responsible for the growth and sustenance of flow-induced vibrations. Based on this recent finding, it is argued that the analysis of the boundary layer separation is sufficient to explain the control mechanism discussed in the current study.

Gaps in the literature: Although some passive boundary-layer control methods including roughness, trip wires and dimples have been studied for a fixed sphere for the purposes of drag reduction, to the authors' knowledge there appears to be no study investigating the effect of such passive control methods on elastically-mounted spheres undergoing flow-induced vibration. A trip wire is perhaps the simplest passive control mechanism imaginable but it is still unknown if it would reduce or enhance flow-induced vibrations of a sphere?

Hypothesis: Based on previous studies on fixed spheres, it is hypothesised that when a sphere is flexibly mounted and undergoing FIV, the delay in flow separation caused by tripping will lead to a reduction in the vibration amplitude. It can be conjectured here based on the prior studies that the trip wire location and size will be the most important characteristic parameters affecting the overall effect on the FIV response. In order to test this hypothesis, we designed a comprehensive series of systematic experiments

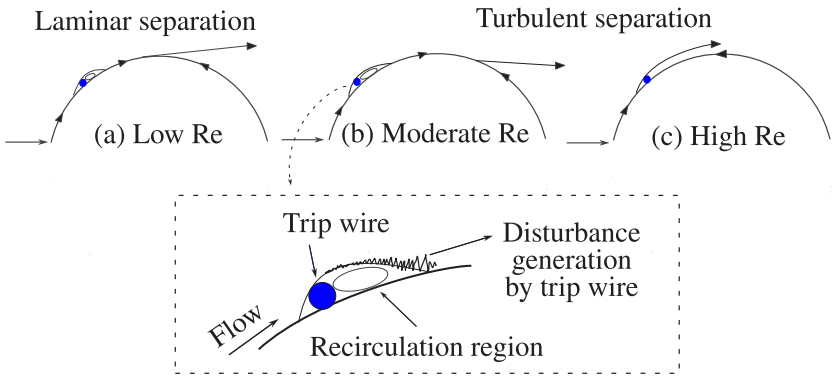

Fig. 1. Schematic of different flow patterns observed in a bluff body (Son et al., 2011 and Igarashi, 1986).

to investigate the effect of tripping the sphere boundary layer on the FIV response for a wide range of trip wire sizes and flow parameters. Since the physical mechanism of delay in flow separation due to the presence of a trip wire for a fixed surface is well documented in the literature, it is not the main focus of this study. The effect of trip wire on the far wake structures will be a part of subsequent future study.

Specific research questions to address: This study advances our fundamental understanding of the effect of tripping the boundary layer on the flow-induced vibration of a three-dimensional bluff body and aims to address the following fundamental questions:

- How does the presence of trip wire affect the flow-induced vibration of an elastically mounted sphere?
- What is the effect of changing the trip wire location?
- How does changing the size of trip wire affect the FIV response of a sphere?
- What is the effect of trip wire on the main flow separation over the sphere? Does the trip wire lead to a narrower near wake?
- Can we use tripping as a passive mechanism to exert control of FIV over a wide Reynolds number range?

In the following sections, we first elaborate on the experimental methods used in the current study (Section 2), followed by a validation study, where the FIV response of a smooth sphere is established (Section 3). In Section 4, the effect of the location of the trip wire is discussed followed by revealing the effect of the trip wire size in Section 5. Finally, the results are summarised and conclusions are drawn in Section 6.

2. Experimental methods

2.1. Details of the fluid–structure interaction system

The response dynamics of flow-induced vibration of bluff bodies is often characterised by the normalised vibration amplitude and frequency response as functions of the reduced velocity, U^*. The normalised amplitude response is defined as $A^* = \sqrt{2}A_{rms}/D$, where A_{rms} is the root-mean-square (rms) oscillation amplitude of the body. The reduced velocity is defined as $U^* = U/f_{\mathrm{nw}}D$, where U is the free stream velocity and f_{nw} is the natural frequency of the system in quiescent water. All other relevant non-dimensional parameters for the current study are listed in Table 1. The governing equation of motion describing the cross-flow motion of the sphere can be written as

$$m\ddot{y} + c\dot{y} + k_s y = F_y, \tag{1}$$

where F_y is the fluid force in the transverse direction, m is the total oscillating mass of the system, y is the displacement in the transverse direction, c is the structural damping of the system, and k_s is the spring constant. As an approximation, it is often assumed that $F_y(t)$ and the response displacement $y(t)$ are both sinusoidal and represented by

$$y(t) = A\sin(2\pi f t), \tag{2}$$

$$F_y(t) = F_o\sin(2\pi f + \phi), \tag{3}$$

where F_o is the amplitude of F_y, and ϕ is the phase between the fluid force and the body displacement.

Based on the suggestions of Lighthill (1986) and as performed for VIV of a tethered sphere by Govardhan and Williamson (2000), the total transverse fluid force (F_y) can be split into a potential force ($F_{\mathrm{potential}}$), comprising the potential added mass force, and a vortex force component (F_{vortex}) that is due to the vorticity dynamics. From the potential theory, the instantaneous $F_{\mathrm{potential}}$ acting on the sphere can be expressed as

$$F_{\mathrm{potential}}(t) = -C_{\mathrm{A}}m_{\mathrm{d}}\ddot{y}(t)\,. \tag{4}$$

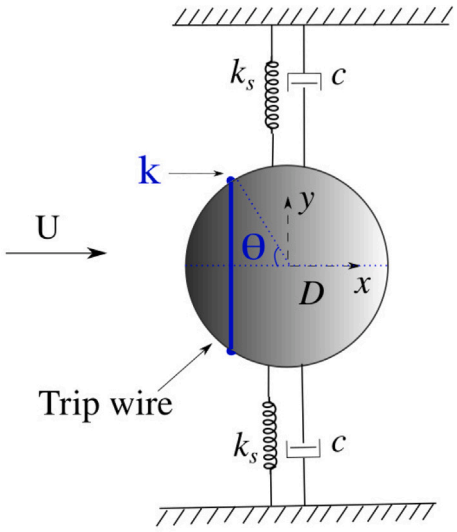

Fig. 2. Definition sketch for the transverse vortex-induced vibration of a sphere with a trip wire. The hydroelastic-system is simplified as a 1-DOF system constrained to move in the cross-flow direction. Here, U is the free-stream velocity, D is the sphere diameter, k_s is the spring constant, c is the structural damping, θ is the location of the trip wire measured from the leading stagnation point to the back of the trip wire, and k is the diameter of the trip wire.

Thus, the vortex force F_{vortex} can be computed from

$$F_{\text{vortex}} = F_y - F_{\text{potential}}\,. \tag{5}$$

If all the forces are normalised by $(\frac{1}{2}\rho U^2 \pi D^2/4)$, this reduces to

$$C_{\text{vortex}}(t) = C_{y_{rms}}(t) - C_{\text{potential}}(t). \tag{6}$$

Here, $C_{\text{potential}}$ (the potential-flow lift coefficient) can be calculated based on the instantaneous body acceleration $\ddot{y}(t)$. Reverting back to the dimensional forces for the moment, two equivalent forms can be written for the equation of motion

$$m\ddot{y} + c\dot{y} + ky = F_o \sin(\omega t + \phi_{\text{total}}), \tag{7}$$

and for vortex force

$$(m + m_{\text{A}})\ddot{y} + c\dot{y} + ky = F_{\text{vortex}} \sin(\omega t + \phi_{\text{vortex}}). \tag{8}$$

The vortex phase ϕ_{vortex}, first introduced by Govardhan and Williamson (2000), is the phase difference between $C_{\text{vortex}}(t)$ and the body displacement $y(t)$. The more conventionally used total phase ϕ_{total} is the phase difference between the total force $C_{y_{rms}}$ and the body displacement $y(t)$. In general, phase jumps are associated with a switch from one VIV mode to another, and have even been used to distinguish between different modes (Govardhan and Williamson, 2005). The instantaneous relative phases between the two forces reported in this paper are calculated using the Hilbert transform as detailed in Khalak and Williamson (1999).

In the present study, the FIV response was studied and characterised over a wide reduced velocity range of $3 \leq U^* \leq 20$ corresponding to the Reynolds number range of $5000 \lesssim Re\ (= U D/\nu) \lesssim 30\,000$, with ν the kinematic viscosity.

2.2. Experimental details

The experiments were conducted in the recirculating free-surface water channel of the Fluids Laboratory for Aeronautical and Industrial Research (FLAIR), Monash University, Australia. The test section of the channel is 600 mm in width, 800 mm in depth and 4000 mm in length. The free stream velocity can be varied in the range of $0.05 \leq U^* \leq 0.45$ m s^{-1}. The free stream turbulence levels in the test section were less than 1% over the velocity range studied.

For a tethered sphere, the maximum vibration amplitude in the streamwise direction is less than 2% of that in the transverse direction. Hence, most of the previous fundamental studies on sphere VIV have focused on studying the vibration response by constraining the sphere motion in the transverse direction only. In the current study, the sphere was elastically mounted in the direction transverse to the oncoming flow using a low-friction air-bearing system that provided low structural damping (see Fig. 2). The structural stiffness was controlled by high quality extension springs. More details of the hydro-elastic facility can be found in Zhao et al. (2018).

Table 1
Non-dimensional parameters used in this study. In this table: A_{rms} is the rms of the vibration amplitude in y transverse direction; D is the sphere diameter; f is the body oscillation frequency; and f_{nw} is the natural frequency of the system in quiescent water. In addition, m is the total oscillating mass; c is the structural damping factor with k_s the spring constant; U is the free-stream velocity; ν is the kinematic viscosity; m_{A} denotes the added mass, defined by $m_{\mathrm{A}} = C_{\mathrm{A}} m_{\mathrm{d}}$, where m_{d} is the mass of the displaced fluid and C_{A} is the potential added mass coefficient (0.5 for a sphere); and F_y is the r.m.s of the fluid force acting on the sphere in the transverse direction.

Amplitude ratio	A^*	$\sqrt{2}A_{rms}/D$
Damping ratio	ζ	$c/\sqrt{k_s(m+m_{\mathrm{A}})}$
Mass ratio	m^*	m/m_{d}
Mass-damping parameter	ξ	$(m^*+C_{\mathrm{A}})\zeta$
Reduced velocity	U^*	$U/(f_{\mathrm{nw}}D)$
Reynolds number	Re	UD/ν
Transverse force coefficient	$C_{y_{rms}}$	$F_y/(\frac{1}{8}\rho U^2\pi D^2)$

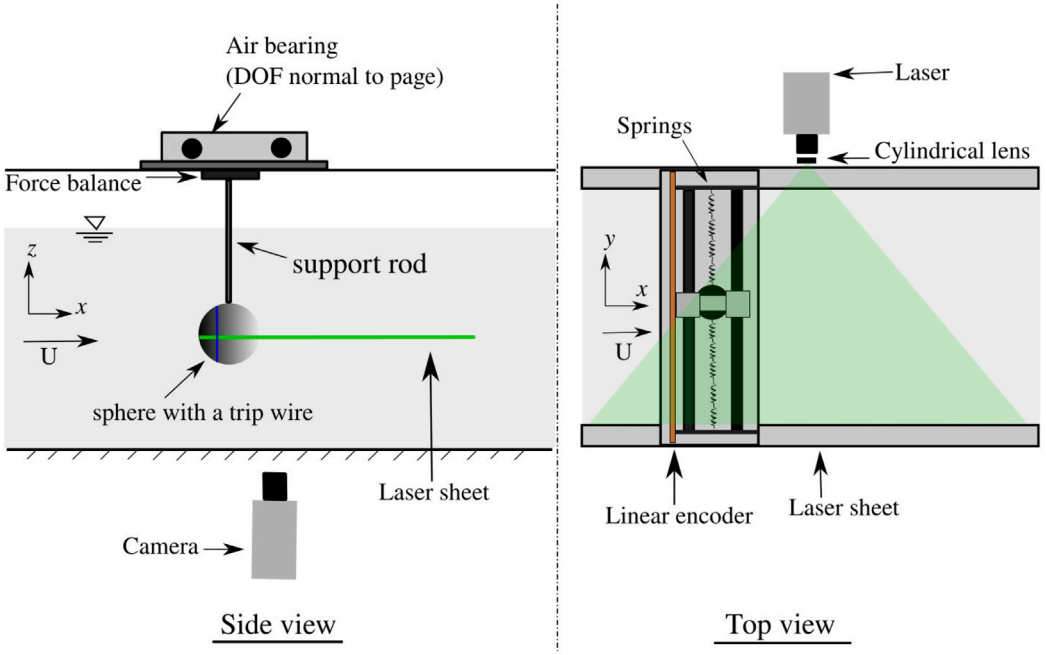

Fig. 3. (Colour online) Schematic (not to scale) showing the experimental setup.

A solid precision-manufactured acrylic sphere of diameter $D = 80$ mm (accuracy within ± 200 μm) was used in the current experiments. The sphere model had a smooth polished surface finish and was supported using a thin cylindrical support rod 3 mm in diameter, manufactured from hardened nitrided stainless steel for extra stiffness and to maintain straightness under FIV oscillations.

The sphere displacement was measured using a linear encoder (model: RGH24, Renishaw, UK) with a resolution of 1 μm. The data acquisition, and the control of the flow velocity and the sphere oscillations were automated via customised LabVIEW programs. For each data set, the signal was acquired at a sampling frequency of 100 Hz for more than 100 vibration cycles. The natural frequencies and structural damping of the system in both air and water were measured by conducting free decay tests individually in air and quiescent water. The natural frequencies in air and water were found to be $f_{na} = 0.249 \pm 0.005$ and $f_{nw} = 0.239 \pm 0.005$. The structural damping ratio in air with consideration of the added mass was determined to be $\zeta = 2.7 \times 10^{-3} \pm 0.0006$. The results in the current study are reported for a mass ratio of $m^* = 7.8$. A brief schematic of the current experimental setup is shown in Fig. 3. Further details of the experimental setup can be found in Sareen et al. (2018c).

In line with the findings proposed by Menon and Mittal (2021), studying the boundary layer separation provides adequate insights into the control mechanism of flow-induced vibration for a bluff body. For a deeper understanding of the control dynamics, we conducted hydrogen-bubble flow visualisations in the x-y plane near the sphere's surface. This allowed us to emphasise both the main flow separation over the sphere surface and the size of the near-wake region. Hydrogen bubbles were generated by an upstream platinum wire 50 μm in diameter and 500 μm in length, which was powered by a potential difference of ∼50 VDC. A laser sheet of ∼3 mm thickness from a continuous laser (model: MLL-N-532-5W, CNI, China), aligned parallel to the x–y plane, was employed to illuminate the bubbles. Imaging was performed using a high-speed camera (model: Dimax S4, PCO, AG) with a resolution of 2016 × 2016 pixels^2. This camera was equipped with a 200 mm Nikon lens.

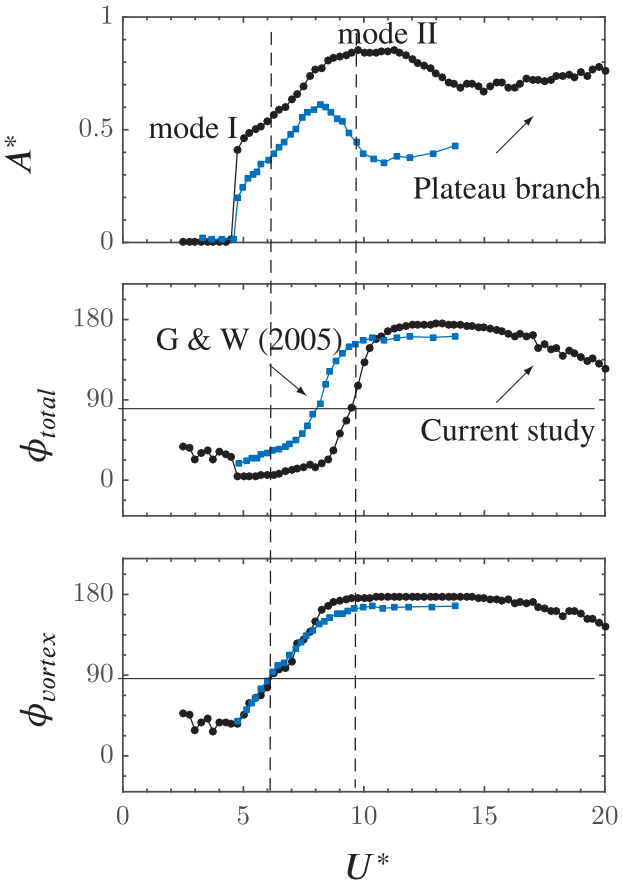

Fig. 4. (Colour online) Variation of the total phase ϕ_{total} (middle) and vortex phase ϕ_{vortex} (bottom) with U^*, correlated with the amplitude response (top). For comparison, the variations reported by Govardhan and Williamson (2005) are also presented (blue square symbols). Mass ratio of the current study is $m^* = 7.8$ compared to 31.3 in their study.

3. VIV response of a sphere without a trip wire

This section provides a brief overview of what is already known about an elastically mounted smooth sphere undergoing VIV. The smooth sphere VIV response has been well documented, and we offer a brief overview of the VIV response for context. Readers are referred to Sareen et al. (2018c) for a more extensive validation study, and to Govardhan and Williamson (2005) for comprehensive previous results.

The typical vibration amplitude response of a sphere with 1-DOF for a low mass-damping parameter of $(m^* + C_A)\zeta = 0.03$ is shown in Fig. 4 in comparison to the study by Govardhan and Williamson (2005) for a relatively high mass-damping parameter of 0.92. The lock-in occurs at a $U^* \approx 4.5$, whereby there is a sudden jump in the sphere vibration amplitude. The vibration amplitude continuously increases from mode I to mode II reaching a peak saturation amplitude of $A^* = 0.8$ at reduced velocity of $ustar \approx 10$. After the peak response, the amplitude response smoothly drops to a lower plateau branch that extends towards mode III as U^* approached 20 (Govardhan and Williamson, 2005; Sareen et al., 2018a,c).

Unlike the case of a tethered sphere with 2-DOF, where the modes are separated by a desynchronised reduced velocity range (Jauvtis et al., 2001; Govardhan and Williamson, 2005), the vibration amplitude for a sphere in the 1-DOF case increases gradually and continuously from mode I to mode II ($4.5 \lesssim U^* \lesssim 15$) leading to an almost constant amplitude in the plateau branch ($15 \leq U^* < 30$). Although it is difficult to demarcate the two modes in the 1-DOF case, there are considerable changes in the phase difference between the sphere displacement and the total transverse force ψ_{total}, and the phase difference between the sphere displacement and the vortex force, ψ_{vortex}. The response transitions from Mode I to Mode II when ψ_{vortex} crosses through 90°, corresponding to the 'inflection point' in the amplitude response. Likewise, within the Mode II regime, ψ_{total} passes continuously through 90°, corresponding to the peak of the amplitude response (Govardhan and Williamson, 2005; Sareen et al., 2018a,c). Lowering the mass-damping parameter $(m^* + C_A)\zeta$ leads to greater vibration amplitudes and a widened synchronisation regime, as shown in Fig. 4. Although the vortex shedding appears fairly similar for all the three vibration modes, there is a change in the timing of the vortex formation in the wake. The vibrations in the 'plateau' region exhibit slight differences to the highly periodic

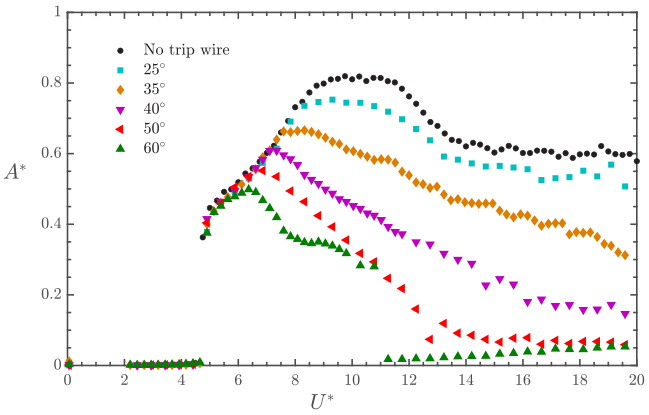

Fig. 5. Variation of A^* with U^* for various trip wire locations. Tripping leads to a reduction in vibration amplitude, particularly at higher reduced velocities. This effect becomes more pronounced as the trip wire is positioned closer to the separation location, indicating a stronger control mechanism. The non-dimensionalised trip wire diameter in this case is $k/D = 0.013$. (For interpretation of the references to colour in this figure legend, the reader is referred to the web version of this article.)

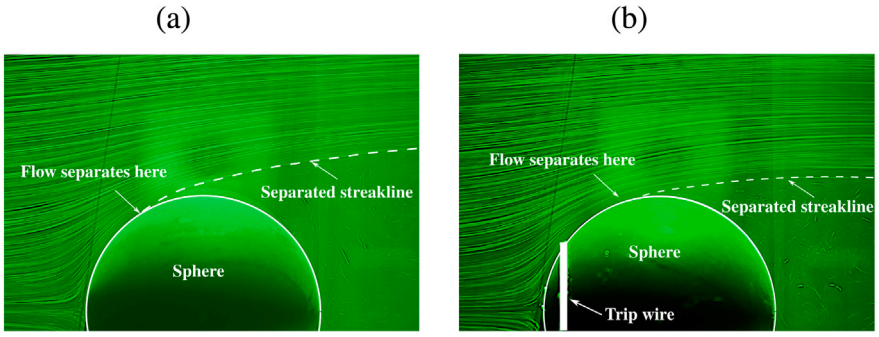

Fig. 6. Hydrogen-bubble visualisation performed for a stationary sphere at high exposure settings to highlight the flow separation location on the sphere surface for (a) smooth sphere at $U^* = 6$, and (b) Sphere with a trip wire of thickness $k/D = 0.013$ located at $\phi = 35°$ at $U^* = 6$. The separating streaklines are highlighted using dashed lines.

vibrations in mode II, albeit, the frequency of oscillation stays close to the natural frequency of the system over the entire U^* range examined in the current study.

4. Effect of the location of the trip wire

In this section, the effect of trip wire location on the VIV response of a sphere is discussed. For this set of experiments, the trip wire thickness was kept constant at $k/D = 0.013$ and the trip wire location ϕ (measured from the leading stagnation point of the sphere) was sequentially varied from 0° (no trip wire) to 60° in small increments.

Fig. 5 shows the variation of non-dimensionalised sphere vibration amplitude A^* with the reduced velocity U^* for various trip wire locations ϕ. For reference, the VIV response of a smooth sphere is also shown (in black circles), whereby the vibrations lock-in at a reduced velocity of $U^* \approx 5$. The VIV response then gradually progresses from mode I to mode II leading to a plateau branch at higher reduced velocities. As evident from the figure, when a trip wire is placed very close to the stagnation point (for example, $\phi = 25°$ shown in cyan square symbols), the bell-shaped response is similar to that of a smooth sphere with slightly reduced vibration amplitude for the mode II and plateau branches. This indicates minimal effect of the perturbations caused by trip wire to the sphere boundary layer when placed very far away from the separation location. Fig. 6 shows the hydrogen-bubble visualisation for a smooth sphere (a) compared with a tripped sphere (trip wire located at $\phi = 35°$) for a reduced velocity of $U^* = 6$ (mode I). It was found that for mode I of the sphere VIV response, the presence of a trip wire of thickness $k/D = 0.013$ does not significantly alter the main flow separation location and the size of the sphere near wake. This finding is consistent with that observed by Son et al. (2011) and Chae et al. (2019) for a fixed sphere with a trip wire. They reported that for low Reynolds numbers, the disturbance induced by the trip wire decays downstream and main separation occurs at a streamwise location similar to that for a stationary smooth sphere. It can be conjectured here that when the sphere is flexibly mounted, a similar mechanism is at play at low Reynolds number, leading to negligible effect of the trip wire on the main separation.

However, when the trip wire is moved further away from the leading stagnation point and closer to the separation location (see $\phi = 35°–60°$), the amplitude response is significantly reduced for mode II. The plateau branch completely disappears at higher

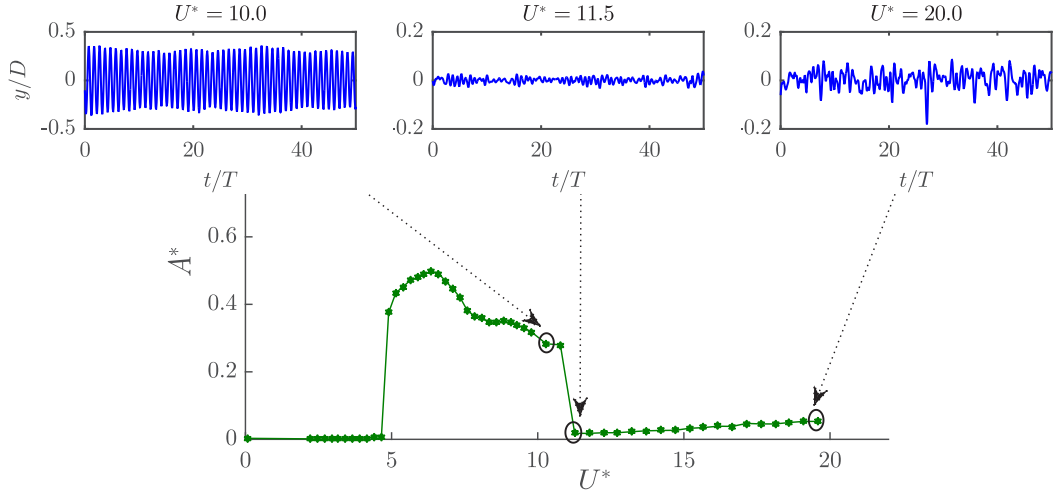

Fig. 7. Variation of A^* with U^* for the trip wire location of $\phi = 60°$. The plots above show time traces of the transverse displacement of the sphere. The vibrations are highly periodic for $U^* < 10$ but show small amplitude chaotic bursts of vibration for $U^* \geq 10$.

reduced velocities. For a given height of the trip, the local boundary layer thickness decreases with an increase in Reynolds number. At high Reynolds number, the disturbance generated by the trip could be large enough to force the boundary layer to undergo direct transition, as shown in Fig. 1(c). Hence, the effect of the trip (and consequently the FIV control) is inherently a strong function of Reynolds number. It can be conjectured here that, perhaps, the attenuation of sphere vibrations at higher reduced velocities is an effect of Reynolds number. Furthermore, as the trip wire is positioned nearer to the separation location, the synchronisation region, characterised by significant vibrations, becomes increasingly narrow. This effect becomes increasingly prominent as the trip wire is located closer to the flow separation. It is important to note here that the sphere mode I VIV response remains unaltered. Moreover, there is no change in the reduced velocity at which lock-in occurs. This is in contrast with that observed for the representative 2-D bluff body prototype — the circular cylinder. Hover et al. (2001) reported an earlier onset of lock-in in the VIV response of a cylinder in the presence of a trip wire.

In the current investigation, the lowest vibration response was observed for $\phi = 60°$, where the vibrations were dramatically suppressed for $U^* > 10$. As evident in the time trace of the displacement signal (Fig. 7), the vibrations are highly periodic for $U^* < 10$, but shows small amplitude bursts of vibration for $U^* \geq 10$. This behaviour is similar to that reported for a circular cylinder. Hover et al. (2001) observed for the case of a circular cylinder undergoing VIV that, at higher reduced velocities (above $U^* \approx 6$), the response is largely eliminated in the presence of the trip wire, and only extremely low fluctuating lift and drag forces remain. For the case of a 3-D bluff body sphere, this dramatic reduction in the vibration amplitude happens at a much higher reduced velocity of $U^* \approx 11$.

Fig. 8 shows hydrogen bubble visualisations for a tripped stationary sphere (located at $\phi = 60°$) at reduced velocities of $U^* = 6$ (a), $U^* = 8$ (b), and $U^* = 11.5$ (c). As evident from the images, there is minimal effect of tripping at $\phi = 60°$ in mode I ($U^* = 6$). However, for mode II, tripping at $\phi = 60°$ leads to significant delay in the main separation. From the images, it is clear that the near wake of the sphere is significantly smaller for $U^* = 8$ compared to that of $U^* = 6$ indicating delay in separation caused by the trip wire. One can deduce here that tripping causes a narrowing of the sphere near wake due to a delay in the overall flow separation. As a result, the transverse fluctuating lift force acting on the sphere is lowered as well, presumably lowering the vibration amplitude. Once the reduced velocity reaches $U^* = 11.5$, there is no further significant delay in the main separation or the near-wake size. This suggests that the drastic decrease in vibration amplitude for $U^* \geq 11.5$ in the plateau branch region for $\phi = 60°$ cannot be attributed solely to the delay in separation caused by the trip wire. The question arises: why are vibrations suppressed for high reduced velocity for $\phi = 60°$? To answer this question, we need to examine the frequency response.

Fig. 9 shows logarithmic-scale power spectra depicting the dominant non-dimensionalised oscillation frequency content, $f^* = f/f_{nw}$, as a function of reduced velocity, correlated with the non-dimensionalised vibration amplitude for $\phi = 35°$ (at the top) and $\phi = 60°$ (at the bottom). The dashed line represents the vortex shedding frequency of a static sphere. For both the trip-wire locations, the dominant vibration frequency remains close to the natural frequency of the system, i.e. $f^* = 1$. For $\phi = 35°$, the vibrations lock-in to the natural frequency at $U^* \approx 5$ and remain locked-in for the entire synchronisation region. However, for $U^* > 14$, where a reduction in the vibration amplitude is observed, there is a relatively broad frequency content in the displacement signal. On the other hand, for the trip-wire location of $\phi = 60°$, there is a clean frequency response in the synchronisation region followed by a dramatic change in the frequency profile of the displacement signal when the vibrations abruptly drop for $U^* \geq 11$, indicating that the vibrations are no longer locked-in. It is clear from the contour of the frequency spectrum plots that within the synchronisation region, the displacement signal shows a clean frequency response with maximum power close to $f^* = 1$. However, a broader range of frequencies is observed outside the synchronisation regime, where small non-periodic vibrations are observed.

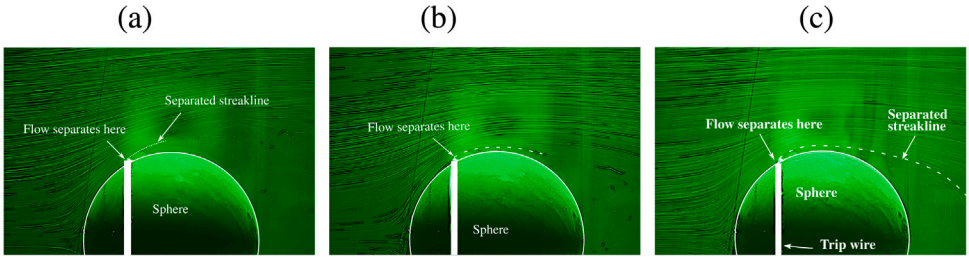

Fig. 8. Hydrogen-bubble visualisation performed for a stationary sphere at high exposure settings to highlight the flow separation location on the sphere surface for (a) $\phi = 60°$ at $U^* = 6$, (b) $\phi = 60°$ at $U^* = 8$, and (c) $\phi = 60°$ at $U^* = 11.5$. The separating streaklines are highlighted using dashed lines. As the reduced velocity is increased, the tripping effects become more pronounced.

Based on these observations, one can deduce that the dramatic reduction in vibration amplitude at high reduced velocities for $\phi = 60°$ is due to the vibrations no longer being locked-in. This is consistent with the findings of Son et al. (2011), who showed that a trip wire may remove coherent frequencies in the wake of a stationary sphere. This suggests that this is the likely reason why the vibrations in this scenario cannot lock-in for large reduced velocities.

Fig. 10 presents a comparison of characteristic vibration parameters between $\phi = 25°$ (left) and $\phi = 60°$ (right). As discussed in Section 3, mode I is distinguished by an abrupt increase in the transverse lift coefficient and a gradual monotonic rise in the vortex phase (ψ_{vortex}) from 0 to 180°. Conversely, during the transition to mode II, there is a small peak observed in c, accompanied by a sharp ascent in the total phase from 0 to 180°. As shown in Fig. 10, both trip-wire locations of $\phi = 25°$ and $\phi = 60°$ show similar characteristics for mode I; in both cases, lock-in occurs at a reduced velocity of approximately $U^* = 5$. However, mode II is initiated much earlier at $U^* = 7$ for $\phi = 60°$ compared to $\phi = 25°$. In addition, for $\phi = 60°$, the entire mode II branch appears to be confined to a narrow range of reduced velocities before a significant decrease in vibration. The pronounced drop in vibration amplitude for $U^* > 10$ correlates with a simultaneous decrease in $C_{y_{rms}}$. Both the vortex and total phases also decrease to 90°. This further provides evidence that vibrations are no longer locked-in for $U^* > 10$.

Overall, it is observed that mode I is robust and impervious to the presence of the perturbations created by the trip wire. For low Reynolds numbers, the disturbance generated by the trip wire is not large enough and decays downstream. However, the trip wire affects the onset of mode II and confines the vibrations to a narrow range of reduced velocities. This is consistent with previous studies that have demonstrated robustness of mode I of the sphere vibration response to various types of external stimuli, such as constant transverse rotation, rotational oscillations or free surface influences (see Sareen et al., 2018a,c,b). If a trip wire is placed fairly close to the separation location, an effective control of the vibration can be achieved in mode II and the plateau branch for high reduced velocities. The control is a strong function of the Reynolds number as the boundary layer thickness decreases with an increase in Reynolds number. The question arises: How can we disrupt mode I of the vibration response? It was hypothesised that using a thicker trip wire may potentially disrupt mode I, but it may introduce an asymmetry in the system that could result in a galloping response at high flow velocities. As the subsequent section will demonstrate, this is precisely what was observed

5. Effect of trip wire thickness

In this section, the effect of trip-wire thickness on the vibration response of a sphere is discussed. Fig. 11 shows the variation of non-dimensionalised vibration amplitude A^*_{rms} with reduced velocity U^* for three different trip-wire thicknesses. As evident from the figure, for a trip wire of thickness $k/D = 0.033$, there is a significant reduction in the vibration amplitude for mode I and II for $U^* \leq 13$. Hydrogen-bubble visualisations shown in Fig. 12 for (a) $k/D = 0.013$ compared to (b) $k/D = 0.033$ at the same values of reduced velocity $U^* = 6$ and location $\theta = 60°$ reveal that the thicker trip wire leads to a significant delay in the main flow separation compared to the thin wire.

However, for $U^* > 13$, the vibration amplitude increases monotonically as a function of reduced velocity indicating a galloping-like response. Galloping is another class of flow-induced vibration observed for bluff bodies with non-circular cross sections (square, triangular, and prism, etc.), whereby the vibrations monotonically increase with the flow velocity until the structural limits are reached. The characteristic feature of a galloping response is that it is typically triggered at relatively very high flow velocities compared to vortex-induced vibration, and that the vibrations occur at lower frequencies relative to the vortex shedding frequency. Frequency content of the sphere displacement signal (not shown here) revealed that the vibrations are still locked to the natural frequency of the system. Since this novel vibration response is triggered within the range of VIV and the vibrations are locked to the natural frequency, it cannot be classified as a (albeit weak) galloping response based on the classic definition. For these reasons, it is referred as galloping-like response in the text here. It is important to note here that this is a different class of flow-induced vibrations different from vortex-induced vibration or galloping. Further research will be needed in the future to completely understand this type of vibration.

If the trip-wire thickness is further increased to $k/D = 0.067$, the galloping-like response is triggered at an even lower reduced velocity of $U^* \approx 8$. Interestingly, there is no change in the reduced velocity where the vibration lock-ins with the natural frequency and it remains at $U^* \approx 5$. We can conclude here that a thicker wire is very effective in suppressing mode I of the vibration response,

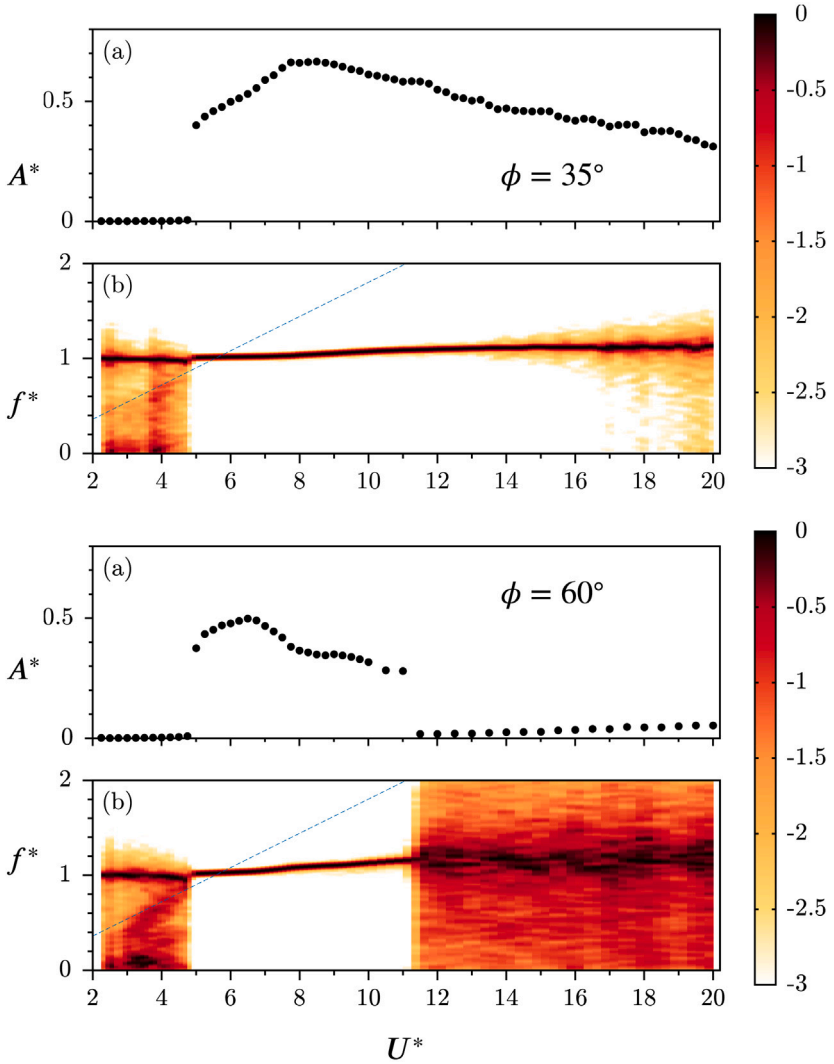

Fig. 9. (Colour online) Power spectral density (PSD) contour plots of the sphere displacement signal as a function of U^* correlated with the amplitude response curve for a trip-wire location of $\phi = 30°$ (above) and $\phi = 60°$ (below). A broad frequency response is observed outside of the synchronisation region. The non-dimensionalised trip-wire thickness here is $k/D = 0.013$.

which is considered the most robust mode of sphere vibration (corresponding to the natural resonance between vortex shedding of a stationary sphere and the system frequency). However, for high reduced velocities, thicker wires may lead to a galloping-like response.

Overall, if the goal of a control application is to exercise vibration suppression, then the thicker wire is effective for lower reduced velocities, however, thinner wires are more useful at higher reduced velocities. On the other hand, if the goal is to harvest renewable energy (thus increase the vibration amplitude and region of synchronisation), then a smooth sphere is needed at low reduced velocities but a thick trip wire for high reduced velocities. The optimum method to exercise an effective control over a wide range of reduced velocity would essentially involve an adaptive trip wire placed close to the separation location that can adapt its thickness with the incoming flow velocity. The discovery that the optimal height of the trip wire for control varies across different flow regimes shares similarities with studies conducted on fixed spheres. In a study by Son et al. (2011), the impact of trip wires on the drag of a fixed sphere was investigated. The study revealed that thicker wires were more effective in reducing drag at low Reynolds numbers, while thinner wires proved more effective at high Reynolds numbers.

6. Conclusions

A systematic set of experiments were undertaken to investigate the effect of tripping the boundary layer on the flow-induced vibration response of a sphere. The response was studied for a wide range of reduced velocities covering $3 \leq U^* \leq 20$, for

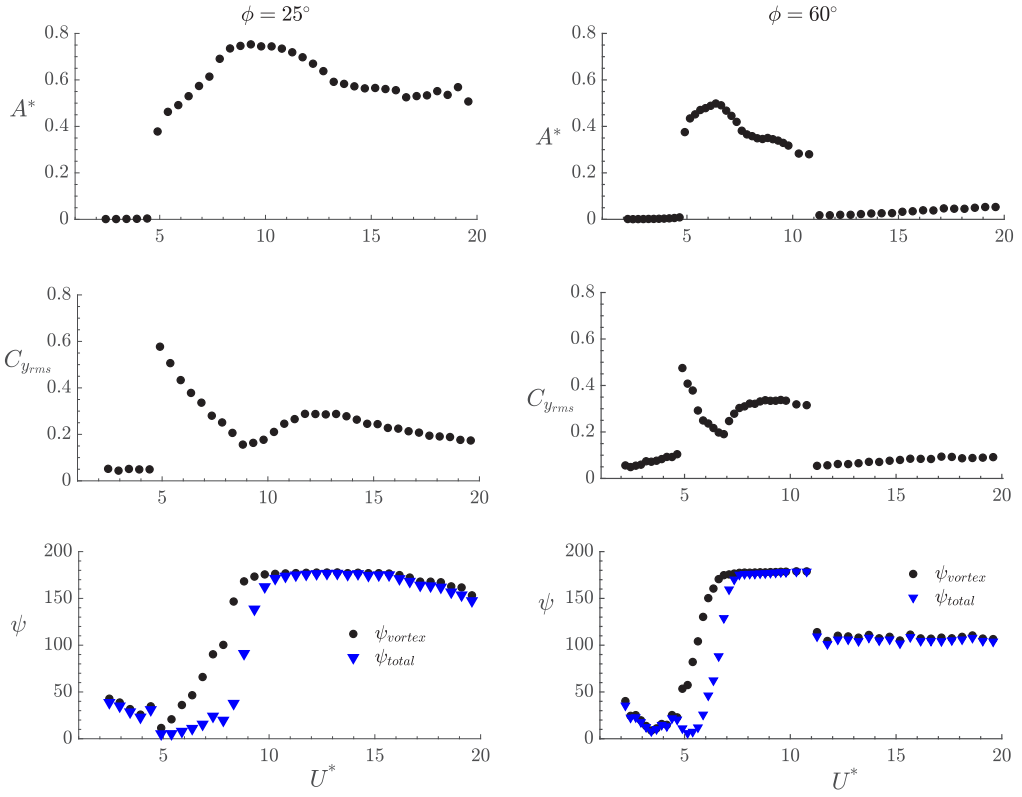

Fig. 10. Comparison of characteristic vibration quantities for $\phi = 25°$ (left) against those for $\phi = 60°$ (right). The figures show the variation of non-dimensionalised vibration amplitude A^*_{rms} (first row), correlated with the fluctuating lift coefficient $C_{y_{rms}}$ (second row), and the vortex/total phase difference (third row) as a function of reduced velocity U^*. The non-dimensionalised trip wire thickness here is $k/D = 0.013$.

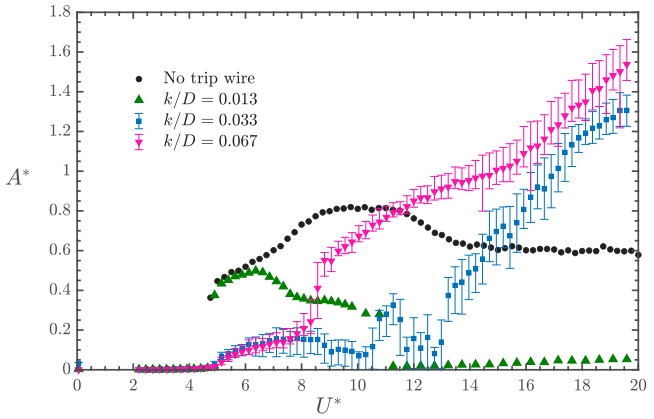

Fig. 11. Variation of A^* with U^* for various trip-wire locations. Thicker trip wires are effective in controlling mode I vibrations but lead to galloping-like response at high reduced velocities. Here, the trip wire was located at $\phi = 60°$.

several trip-wire locations ϕ = 25°–60° and sizes k/D = 0.013–0.067. It was found that as the trip wire is placed closer and closer to the (smooth-surface) separation location of the 3D boundary layer, the vibration response progressively decreases and the synchronisation region narrows. The trip-wire control is effective in suppressing vibration for the mode II and plateau branch responses. However, Mode I is robust and remains relatively impervious to disturbances induced by thin trip wires. Interestingly, the lock-in first occurs at the same reduced velocity for all the locations of the trip wire, which is in contrast with that observed previously for a 2D bluff body – a circular cylinder. Thicker trip wires can disrupt mode I but excite a (weak) galloping-type response at higher reduced velocity.

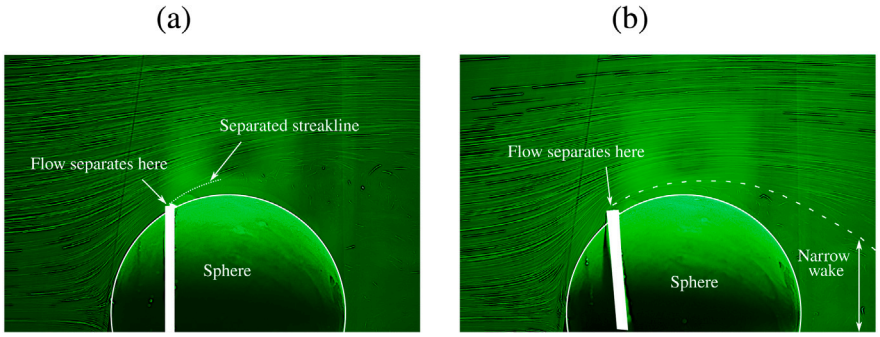

Fig. 12. Hydrogen-bubble visualisations performed for a stationary sphere highlighting the flow separation location on the sphere surface for (a) $\phi = 60°$ at $U^* = 6$ for a trip wire of thickness of $k/D = 0.013$, and (b) $\phi = 60°$ at $U^* = 6$ for a trip wire of thickness of $k/D = 0.033$. Approximate separating streaklines are highlighted using dashed lines. The presence of a thicker trip wire results in a noticeable delay in the main flow separation.

In conclusion, tripping proves to be an effective passive flow control method for controlling flow-induced vibration response in 3D bluff bodies when strategically positioned. However, there is no universal optimal size for the trip wire that ensures effective control across the entire range from mode I to the plateau branch. While thicker wires suppress mode I, thinner wires are required for controlling mode II and the plateau branch. To address this limitation, future work should focus on designing an adaptive mechanism where the trip wire can adjust its size based on the flow velocity to achieve desired control throughout the entire range of reduced velocities.

It should be noted that an inherent limitation of this mechanism is the need to position the trip wire in close proximity to the separation location. Additionally, at high reduced velocities, the flow characteristics exhibit notable sensitivity to angular biases, as also observed in studies involving trip wires on cylinders. Subsequent investigations should delve into the underlying causes of these biases and devise strategies to mitigate their impact.

The results of this research represent a significant advancement in our fundamental understanding of utilising a passive triggering mechanism, such as a trip wire, for controlling flow-induced vibrations in three-dimensional bluff bodies. These findings have practical implications for enhancing the performance of renewable energy converters that rely on flow-induced vibrations for energy harvesting. Moreover, the research outcomes can be employed to effectively suppress these vibrations, leading to reduced maintenance costs for offshore structures. Additionally, the findings have potential applications in improving the aerodynamic or hydrodynamic efficiency of unmanned aerial vehicles (UAVs) and micro autonomous underwater vehicles (AUVs). Overall, this research provides valuable insights with broad implications across various domains.

CRediT authorship contribution statement

Anchal Sareen: Conceptualization, Data curation, Formal analysis, Investigation, Methodology, Validation, Visualization, Writing – original draft, Writing – review & editing. **Kerry Hourigan:** Conceptualization, Formal analysis, Funding acquisition, Investigation, Methodology, Project administration, Resources, Software, Supervision, Writing – review & editing. **Mark C. Thompson:** Conceptualization, Formal analysis, Funding acquisition, Investigation, Methodology, Project administration, Resources, Software, Supervision, Writing – review & editing.

Declaration of competing interest

The authors declare that they have no known competing financial interests or personal relationships that could have appeared to influence the work reported in this paper.

Data availability

Data will be made available on request.

Acknowledgment

Authors acknowledge the support from grants DP150102879 and LE170100203.

References

Achenbach, E., 1972. Experiments on the flow past spheres at very high Reynolds numbers. J. Fluid Mech. 54 (3), 565–575.

Achenbach, E., 1974. The effects of surface roughness and tunnel blockage on the flow past spheres. J. Fluid Mech. 65 (1), 113–125.

Alam, M.M., Zhou, Y., Zhao, J., Flamand, O., Boujard, O., 2010. Classification of the tripped cylinder wake and bi-stable phenomenon. Int. J. Heat Fluid Flow 31 (4), 545–560.

Anderson, E., Szewczyk, A., 1997. Effects of a splitter plate on the near wake of a circular cylinder in 2 and 3-dimensional flow configurations. Exp. Fluids 23 (2), 161–174.

Bearman, P.W., 1984. Vortex shedding from oscillating bluff bodies. Annu. Rev. Fluid Mech. 16 (1), 195–222.

Bearman, P., Harvey, J., 1993. Control of circular cylinder flow by the use of dimples. AIAA J. 31 (10), 1753–1756.

Behara, S., Mittal, S., 2011. Transition of the boundary layer on a circular cylinder in the presence of a trip. J. Fluids Struct. 27 (5–6), 702–715.

Blackburn, H., Melbourne, W., 1996. The effect of free-stream turbulence on sectional lift forces on a circular cylinder. J. Fluid Mech. 306, 267–292.

Blevins, R.D., 1990. Flow-Induced Vibration, second ed. Krieger Publishing Company, Malabar, p. 377.

Chae, S., Lee, S., Kim, J., Lee, J.H., 2019. Adaptive-passive control of flow over a sphere for drag reduction. Phys. Fluids 31 (1), 015107.

Choi, J., Jeon, W., Choi, H., 2006. Mechanism of drag reduction by dimples on a sphere. Phys. Fluids 18 (4), 041702.

Choi, H., Jeon, W., Kim, J., 2008. Control of flow over a bluff body. Annu. Rev. Fluid Mech. 40, 113–139.

Dalton, C., Xu, Y., Owen, J., 2001. The suppression of lift on a circular cylinder due to vortex shedding at moderate Reynolds numbers. J. Fluids Struct. 15 (3–4), 617–628.

Deshpande, R., Shakya, R., Mittal, S., 2018. The role of the seam in the swing of a cricket ball. J. Fluid Mech. 851, 50–82.

Ekmekci, A., Rockwell, D., 2010. Effects of a geometrical surface disturbance on flow past a circular cylinder: a large-scale spanwise wire. J. Fluid Mech. 665, 120–157.

Govardhan, R., Williamson, C., 2000. Modes of vortex formation and frequency response of a freely vibrating cylinder. J. Fluid Mech. 420, 85–130.

Govardhan, R., Williamson, C., 2005. Vortex-induced vibrations of a sphere. J. Fluid Mech. 531, 11–47.

Güven, O., Farell, C., Patel, V.C., 1980. Surface-roughness effects on the mean flow past circular cylinders. J. Fluid Mech. 98 (4), 673–701.

Hover, F., Tvedt, H., Triantafyllou, M., 2001. Vortex-induced vibrations of a cylinder with tripping wires. J. Fluid Mech. 448, 175–195.

Hwang, J., Yang, K., Sun, S., 2003. Reduction of flow-induced forces on a circular cylinder using a detached splitter plate. Phys. Fluids 15 (8), 2433–2436.

Igarashi, T., 1986. Effect of tripping wires on the flow around a circular cylinder normal to an airstream. Bull. JSME 29 (255), 2917–2924.

Jauvtis, N., Govardhan, R., Williamson, C., 2001. Multiple modes of vortex-induced vibration of a sphere. J. Fluids Struct. 15 (3–4), 555–563.

Khalak, A., Williamson, C.H., 1999. Motions, forces and mode transitions in vortex-induced vibrations at low mass-damping. J. Fluids Struct. 13 (7–8), 813–851.

Kiya, M., Suzuki, Y., Arie, M., Hagino, M., 1982. A contribution to the free-stream turbulence effect on the flow past a circular cylinder. J. Fluid Mech. 115, 151–164.

Kwon, K., Choi, H., 1996. Control of laminar vortex shedding behind a circular cylinder using splitter plates. Phys. Fluids 8 (2), 479–486.

Lee, S., Kim, H., 1997. The effect of surface protrusions on the near wake of a circular cylinder. J. Wind Eng. Ind. Aerodyn. 69, 351–361.

Lighthill, J., 1986. Fundamentals concerning wave loading on offshore structures. J. Fluid Mech. 173, 667–681.

Lim, H., Lee, S., 2002. Flow control of circular cylinders with longitudinal grooved surfaces. AIAA J. 40 (10), 2027–2036.

Maxworthy, T., 1969. Experiments on the flow around a sphere at high Reynolds numbers. J. Appl. Mech. Trans. ASME E 36, 598–607.

McQueen, T., Zhao, J., Sheridan, J., Thompson, M., 2020. Feedback control of flow-induced vibration of a sphere. J. Fluid Mech. 889, A30.

Menon, K., Mittal, R., 2021. On the initiation and sustenance of flow-induced vibration of cylinders: insights from force partitioning. J. Fluid Mech. 907, A37.

Naudascher, E., Rockwell, D., 2012. Flow-Induced Vibrations: An Engineering Guide. Courier Corporation, p. 432.

Ozono, S., 1999. Flow control of vortex shedding by a short splitter plate asymmetrically arranged downstream of a cylinder. Phys. Fluids 11 (10), 2928–2934.

Païdoussis, M.P., Price, S., De Langre, E., 2010. Fluid-Structure Interactions: Cross-Flow-Induced Instabilities. Cambridge University Press.

Sakamoto, H., Haniu, H., 1994. Optimum suppression of fluid forces acting on a circular cylinder. J. Fluids Eng. 221–227.

Sareen, A., Zhao, J., Jacono, D.L., Sheridan, J., Hourigan, K., Thompson, M.C., 2018a. Vortex-induced vibration of a rotating sphere. J. Fluid Mech. 837, 258–292.

Sareen, A., Zhao, J., Sheridan, J., Hourigan, K., Thompson, M., 2018b. The effect of imposed rotary oscillation on the flow-induced vibration of a sphere. J. Fluid Mech. 855, 703–735.

Sareen, A., Zhao, J., Sheridan, J., Hourigan, K., Thompson, M., 2018c. Vortex-induced vibrations of a sphere close to a free surface. J. Fluid Mech. 846, 1023–1058.

Sareen, A., Zhao, J., Sheridan, J., Hourigan, K., Thompson, M.C., 2019. Large amplitude cross-stream sphere vibration generated by applied rotational oscillation. J. Fluids Struct. 89, 156–165.

Sarpkaya, T., 2004. A critical review of the intrinsic nature of vortex-induced vibrations. J. Fluids Struct. 19 (4), 389–447.

Shih, W., Wang, C., Coles, D., Roshko, A., 1993. Experiments on flow past rough circular cylinders at large Reynolds numbers. J. Wind Eng. Ind. Aerodyn. 49 (1–3), 351–368.

Son, K., Choi, J., Jeon, W., Choi, H., 2011. Mechanism of drag reduction by a surface trip wire on a sphere. J. Fluid Mech. 672, 411–427.

Strykowski, P.J., Sreenivasan, K.R., 1990. On the formation and suppression of vortex 'shedding'at low Reynolds numbers. J. Fluid Mech. 218, 71–107.

Williamson, C.H.K., Govardhan, R., 2004. Vortex-induced vibrations. Annu. Rev. Fluid Mech. 36 (1), 413–455.

Zhao, J., Jacono, D.L., Sheridan, J., Hourigan, K., Thompson, M.C., 2018. Experimental investigation of in-line flow-induced vibration of a rotating circular cylinder. J. Fluid Mech. 847, 664–699.